Physics-informed neural networks for quantum control

Ariel Norambuena,[1, *] Marios Mattheakis,[2] Francisco J. González,[1] and Raúl Coto[1, †]

[1]*Centro de Investigación DAiTA Lab, Facultad de Estudios Interdisciplinarios, Universidad Mayor, Chile*
[2]*John A. Paulson School of Engineering and Applied Sciences,*
Harvard University, Cambridge, Massachusetts 02138, USA
(Dated: June 14, 2022)

Quantum control is a ubiquitous research field that has enabled physicists to delve into the dynamics and features of quantum systems. In addition to steering the system, quantum control has delivered powerful applications for various atomic, optical, mechanical, and solid-state systems. In recent years, traditional control techniques based on optimization processes have been translated into efficient artificial intelligence algorithms. Here, we introduce a computational method for optimal quantum control problems via physics-informed neural networks (PINNs). We apply our methodology to open quantum systems by efficiently solving the state-to-state transfer problem with high probabilities, short-time evolution, and minimizing the power of the control. Furthermore, we illustrate the flexibility of PINNs to solve the same problem under changes in parameters and initial conditions, showing advantages in comparison with standard control techniques.

Introduction.— Optimal Quantum Control (QC) is crucial to exploit all the advantages of quantum systems, ranging from entangled states preparation and quantum registers to quantum sensing. Nowadays, QC can be achieved by means of controllable dissipative dynamics [1, 2], measurement-induced backaction [3–5], Lyapunov control [6, 7], and optimal pulse sequences [8]. These QC techniques serves multiple purposes including state preservation, state-to-state transfer [9], dynamical decoupling in open systems [10–12] and trajectory tracking [13, 14]. Furthermore, we have witnessed powerful applications across multiple platforms including atomic systems [16, 17], light-matter systems [18, 19], solid-state devices [20, 21], trapped ions [22], among other. Dynamical QC stems from a time-dependent Hamiltonian that steers the dynamics [26], and it is subjected to several constraints like laser power, inhomogeneous frequency broadening, and relaxation processes, to name a few. Therefore, finding the optimal sequence for QC is highly cumbersome, and generally, it depends on the particular system.

Complex computational calculations are at the forefront of numerical methods to tackle down simulation of quantum systems. For instance, a parametrization of quantum states in terms of neural networks has enabled the approximation of many-body wavefunctions in closed dynamics (dissipation free) [28–30], and it has also been extended to approach the density operator in open dynamics (dissipative) [31–36]. These approaches use restricted Boltzmann machine parametrization, stochastic reconfiguration, and variational Monte Carlo. Along these ideas, other models have focused on hybrid implementations [37–39], probabilistic formulations based on positive operator-valued measure [40, 41], or data-driven model via time-averaged generators [42]. Overall, estimating the open dynamics of a quantum system is a challenging problem. Beyond this point, one may wonder how evolution can be controlled using a universal and robust approach. Here, machine learning provides versatile and promising algorithms to expand our alternatives towards completing this task [50–56]. However, combining
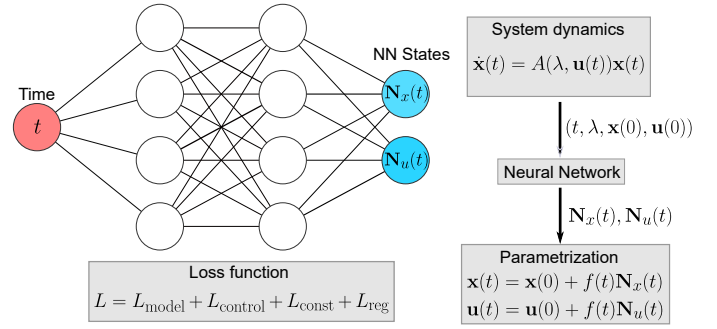

FIG. 1. PINNs architecture for solving inverse quantum control problems. Quantum evolution can be translated into a dynamical system $\dot{\mathbf{x}}(t) = A(\lambda, \mathbf{u}(t))\mathbf{x}(t)$, where $\mathbf{x}(t)$ and $\mathbf{u}(t)$ are the state and control vectors, respectively, and λ are the system parameters. The input data (red circle) is given by the discrete time vector t, and the outputs of the neural network (NN) are $\mathbf{N}_x(t)$ and $\mathbf{N}_u(t)$ (blue circle). By minimizing the loss function L the NN discover $\mathbf{N}_{x,u}(t)$ for the parameterized solutions $\mathbf{x}(t)$ and $\mathbf{u}(t)$, where $f(0) = 0$.

time evolution and QC, being solved within a single deep learning method remains relatively unexplored. The formulation of the QC problem leads us to a non-homogeneous set of differential equations that we aim to solve in an unsupervised yet ansatz-free formalism.

Neural Networks (NNs) are commonly trained with data allowing them to learn the dynamics of the quantum system. However, NNs that preserve the underlying physical laws without preliminary data would have practical advantages. Hence, physics-informed neural networks (PINNs) have been introduced as a new artificial intelligence paradigm that only requires the model itself [68, 69]. This is a general physics-informed machine learning framework that has been applied to solve high-dimensional partial differential equations [70, 71], quantum systems with many-body electronic interactions [72], inverse problems using sparse and noisy data [73], and to discover underlying physics hidden in data structures [74]. Since PINNs

are coded using physical laws, they can be applied to any quantum evolution where the model is well known [60–65].

In this letter, we introduce a novel PINN architecture to find optimal control functions in open quantum systems. This is a data-free inverse modeling deep learning approach where we have a target dynamical behavior instead of data. Our approach suggests smooth control functions for driving the quantum system to a pre-selected target state.

Control theory and physics-informed neural networks.— Let us consider the following n-dimensional non-autonomous dynamical system:

$$\dot{\mathbf{x}} = A(\lambda, \mathbf{u}(t))\mathbf{x}(t), \quad \mathbf{x}(0) = \mathbf{x}_0, \quad \mathbf{u}(0) = \mathbf{u}_0, \quad (1)$$

where $\mathbf{x}(t) = (x_1, ..., x_n)^T \in \mathbb{R}^n$, $\mathbf{u}(t) = (u_1, ..., u_m)^T \in \mathbb{R}^m$, and $\lambda = (\lambda_1, ..., \lambda_s)^T \in \mathbb{R}^s$ are the state, control, and parameter vectors (with $n, m, s \geq 1$ and $m \leq n^2$), respectively. Here, $A(\lambda, \mathbf{u}(t))$ is a real $n \times n$ dynamical matrix that depends on $\mathbf{u}(t)$ and λ.

Given a dynamical system with known λ and with $\mathbf{x}(t)$ satisfying Eq. (1), we can employ machine learning to discover an optimal control vector $\mathbf{u}(t)$ such that the system evolves from $\mathbf{x}(0)$ to some desired target state $\mathbf{x}_d$. Well-known techniques based on optimal control [27], Lyapunov control theory [6] or linear control theory are based on optimization rules to find a suitable control vector $\mathbf{u}(t)$. Therefore, the main idea is to construct a PINN that minimizes a generic loss function to achieve optimal quantum control.
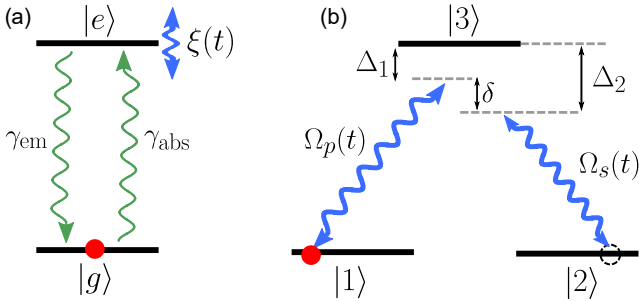

FIG. 2. (a) Open two-level system controlled by a time-dependent atomic modulation $\xi(t)$. Losses are included through absorption (γ_{abs}) and emission (γ_{em}) processes. (b) Open three-level Λ system controlled by two driving fields $\Omega_p(t)$ and $\Omega_s(t)$. We include pure dephasing rates γ_i ($i = 1, 2, 3$) acting on each state $|i\rangle$. One- ($\Delta_{1,2}$) and two-photon (δ) detunings are considered in our numerical simulations.

A feed forward NN is known for being a powerful universal approximator. In other words, it can properly approximate any vector function $F : \mathbb{R}^p \mapsto \mathbb{R}^q$ ($r, q \geq 1$), which is granted by the universal approximation Theorem [75]. Let us consider the NN architecture illustrated in Fig. 1. We have set a time array $t = (t_1, ..., t_M)$ as the input to the neural network, with M representing the dimension of the sample points. We remark that PINNs do not required a structured mesh and thus, t_i can be arbitrary discretized. The NN consists of multiple hidden layers with trigonometric $\sin(\cdot)$ function used as the activation function for

the hidden neurons. This choice of activation has been shown to improve PINNs' performance in solving nonlinear dynamical systems [76] and high-dimensional partial differential equations [71]. The outputs of the NN are the solutions $\mathbf{N}_x(t) \in \mathbb{R}^n$ and $\mathbf{N}_u(t) \in \mathbb{R}^m$. We construct a neural state and control vectors that identically satisfies the initial conditions by parametrizing $\mathbf{x}(t) = \mathbf{x}(0) + f(t)\mathbf{N}_x(t)$ and $\mathbf{u}(t) = \mathbf{u}(0) + f(t)\mathbf{N}_u(t)$, where $f(t) = 1 - e^{-t}$ is a parametric function satisfying $f(0) = 0$ [76]. The network parameters, weights and biases, are randomly initialized and then, they are optimized by minimizing a physics-informed loss function defined by

$$L = L_{\mathrm{model}} + L_{\mathrm{control}} + L_{\mathrm{const}} + L_{\mathrm{reg}}. \quad (2)$$

The component L_{model} describes the system dynamics:

$$L_{\mathrm{model}} = \sum_{i=1}^{M} ||\dot{\mathbf{x}}(t_i) - A(\lambda, \mathbf{u}(t_i))\mathbf{x}(t_i)||^2, \quad (3)$$

with $||\cdot||$ representing a Euclidean distance. The time derivatives in the neural solutions are computed using the automatic differentiation method provided by PyTorch package [78]. By minimizing the above functional, the state vector will approximately satisfy the system dynamics and, thus, the underlying physics. The second term on the right-hand side of Eq. (2) represents the control, that reads

$$L_{\mathrm{control}} = \eta \sum_{i=1}^{M} ||\mathbf{x}(t_i) - \mathbf{x}_d||^2, \quad 0 \leq \eta \leq 1, \quad (4)$$

where the factor η regulates the relevance of the control condition compared to the leading loss component L_{model}. Note that $\mathbf{x}_d$ could be a constant (regulation) or time-dependent (trajectory tracking) vector depending on the control scheme — the proposed method is valid for both schemes. The term L_{const} takes into account additional physical constraints for the state/control vector, respectively, such as probability conservation or holonomic constraints of the form $H(\mathbf{x}, \mathbf{u}, t) = 0$. Finally, L_{reg} is a standard regularization loss term that encourages the network parameters to take relatively small values avoiding overfitting. In this data-free machine learning approach, the effect of overfitting will be the prediction of a too complex $\mathbf{u}(t)$, which might be practically unfeasible. We introduce L_{reg} as a l_2-norm of the network weights $L_{\mathrm{reg}} = \chi \sum_i \mathrm{w}_i^2$, where χ is the regularization parameter.

The minimization of the physics-informed loss function given in Eq. (2) yields NN predictions that obey the underlying physics and suggest optimal control functions. For the training of the NN, namely, to minimize Eq. (2), we employ Adam optimizer [77]. Moreover, the points t_i are randomly perturbed during training iteration— this method has been shown to improve the training and the neural predictions [70, 76].

Two-level system with amplitude damping and one control field.— We consider a two-level system as a proof-of-principle example to illustrate the power of PINNs for QC. In particular, we address the problem of generating Gibbs (mixed) states of the form $\rho_{\text{Gibbs}} = Z^{-1} \sum_j e^{-\beta E_j} |j\rangle\langle j|$ with $Z = \text{Tr}(e^{-\beta H})$ (partition function) and $\beta = (k_B T)^{-1}$ (inverse temperature). The preparation of mixed states is relevant for simulating high-temperature superconductivity in variational quantum circuits [80]. In addition, QC of two-level systems is also relevant in the context of pulse reverse engineering [79], feedback control [3], optimal control theory [27], and controllable quantum dissipative dynamics [43]. Let us consider the following Hamiltonian:

$$H(t) = \omega_z \sigma_z + \omega_x \sigma_x + \xi(t)\sigma_{ee}, \qquad (5)$$

with $\omega_{x,z}$ representing system parameters and $\xi(t)$ describing the unknown control field. Here, $\sigma_z = |e\rangle\langle e| - |g\rangle\langle g|$ and $\sigma_x = |e\rangle\langle g| + |g\rangle\langle e|$, with $|e\rangle$ ($|g\rangle$) being the excited (ground) state. The control relies on the atomic modulation $\xi(t)$ to drive the system towards any desired Gibbs state. Furthermore, we consider an open dynamics described by the Markovian master equation $\dot{\rho} = -i[H(t), \rho] + \sum_{i=1,2} \gamma_i (L_i \rho L_i^\dagger - (1/2)\{L_i^\dagger L_i, \rho\})$, with $[\cdot, \cdot]$ and $\{\cdot, \cdot\}$ representing the commutator and anticommutator, respectively. The dissipation is described by absorption ($L_1 = |e\rangle\langle g|$) and emission ($L_2 = |g\rangle\langle e|$) processes with rates $\gamma_1 = \gamma_{\text{abs}}$ and $\gamma_2 = \gamma_{\text{em}}$, respectively. A schematic representation of the system is given in Fig. 2-(a). In what follows, we use the system parameters $\omega_z = 2$, $\omega_x = 1$, $\gamma_{\text{abs}} = 0.1$, $\gamma_{\text{em}} = 0.3$, and the initial condition $\xi(0) = 0$. For $\xi(t) = 0$, a straightforward calculation leads to the steady-state $\rho^{\text{ss}} = 0.2775|e\rangle\langle e| + 0.7225|g\rangle\langle g| + [(-0.1106 + i0.0083)|g\rangle\langle e| + c.c]$. Thus, we use $\xi(t)$ to drive the system to another stationary state, say, $\rho_d = (1/2)(|e\rangle\langle e| + |g\rangle\langle g|)$. The proposed PINN handles only real-valued functions. Hence, to implement our PINN scheme, we introduce the real state vector $\mathbf{x}(t) = (x_1, x_2, x_3, x_4)^T = (\rho_{gg}, \rho_{ee}, \text{Re}(\rho_{eg}), \text{Im}(\rho_{eg}))^T$, where $\rho_{ij} = \langle i|\rho(t)|j\rangle$ are the elements of the density matrix. Hence, the dynamics can be written as $\dot{\mathbf{x}} = A(\lambda, \mathbf{u}(t))\mathbf{x}(t)$, with

$$A(\lambda, \mathbf{u}(t)) = \begin{pmatrix} -\gamma_{\text{abs}} & \gamma_{\text{em}} & 0 & -2\omega_x \\ \gamma_{\text{abs}} & -\gamma_{\text{em}} & 0 & 2\omega_x \\ 0 & 0 & -\Gamma & -2\omega_z - \xi(t) \\ \omega_x & -\omega_x & 2\omega_z + \xi(t) & -\Gamma \end{pmatrix}, \qquad (6)$$

where $\lambda = (w_x, w_z, \gamma_{\text{abs}}, \gamma_{\text{em}})$ is the set of known parameters, $\mathbf{u}(t) = \xi(t)$ is the one-dimensional control vector that needs to be discovered, and $\Gamma = (1/2)(\gamma_1 + \gamma_2)$ is the effective dephasing rate. The implementation of the loss function and dynamical analysis of the system is described in the Supplemental Material [81]. Hereafter, we use the predicted control function to simulate the dynamics in a standard integrator. In Fig. 3 we plot the dynamics using the PINN's prediction for the control $\xi(t)$ (inset). The PINN
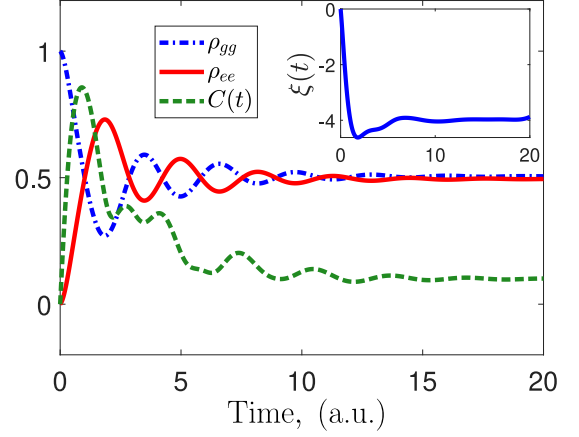

FIG. 3. Controlled dynamics for populations $\rho_{gg}(t)$, $\rho_{ee}(t)$ and quantum coherence $C(t)$ for the control function $\xi(t)$ predicted by the PINN. The architecture of the NN consists of 4 hidden layers of 200 neurons, it is trained for 4×10^4 epochs with a learning rate 10^{-4}, $\chi = 10^{-3}$, and $\eta = 1$.

discovers an optimal Gibbs state preservation with fidelity $F(\rho(t), \rho_d) = [\text{Tr}(\rho^{1/2}(t)\rho_d\rho^{1/2}(t))]^2 = 0.99$ (for $t \geq 20$), and the steady-state approaches to ρ_d within an error of 1% for each component of the density matrix [81]. We remark that our result outperforms the analytically optimized solution that finds $\rho_{gg}^{\text{ss}} = 0.549$, $\rho_{ee}^{\text{ss}} = 0.4510$, $\text{Re}(\rho_{eg}) = 0$, and $\text{Im}(\rho_{eg}) = 0.049$, for a constant control $\xi^{\text{ss}} = -4$ (see [81] for further details). The latter explains the asymptotic behavior for $\xi(t)$ predicted by the PINN. Moreover, we note in Fig. 3 that the quantum coherence $C(t) = 2|\rho_{eg}(t)|$ is highly activated during the transient dynamics in order to generate an equally distributed mixed state, but it asymptotically reaches $C \approx 0.1014$.

Three-level system.— We now explore a more complex scenario that encompasses a three-level system interacting with two control fields. We focus on a Λ-configuration shown by Fig. 2-(b), which has been of paramount importance for the study of quantum effects like electromagnetically induced transparency [44, 45], coherent population trapping [46, 47] and adiabatic population transfer [48]. The latter, has been dubbed Stimulated Raman Adiabatic Passage (STIRAP) [49] and it will be our main point for comparison. Let's begin with the system Hamiltonian $H = \sum_i E_i \sigma_{ii} + H_c(t)$, where E_i stands for the eigenenergies $\sigma_{ij} = |i\rangle\langle j|$, and $H_c(t)$ is the control Hamiltonian. In a multi-rotating frame and after the rotating wave approximation, the dynamics of the three-level system is governed by ($\hbar = 1$):

$$H(t) = \delta\sigma_{22} + \Delta_1\sigma_{33} + \left(\frac{\Omega_p(t)}{2}\sigma_{31} + \frac{\Omega_s(t)}{2}\sigma_{32} + h.c.\right), \qquad (7)$$

where $\Delta_1 = E_3 - E_1 - \omega_p$ and $\Delta_2 = E_3 - E_2 - \omega_s$ are the one-photon detunings that originate from off-resonant driving fields with frequencies ω_p and ω_s, while $\delta = \Delta_1 - \Delta_2$ is the two-photon detuning. Here, $\Omega_p(t)$ and $\Omega_s(t)$ are the

control fields to be found. A similar Hamiltonian can be obtained from the interaction of a Nitrogen-Vacancy center with a Carbon-13 nuclear spin [84, 85]. In what follows, we showcase our population transfer problem to be solved by PINNs. We aim to find the optimal control pulses ($\Omega_p(t)$ and $\Omega_s(t)$) to transfer population from state $|1\rangle$ to state $|2\rangle$ via the lossy intermediary state $|3\rangle$. Our goal is to train a PINN that completes the task reaching high fidelity, with (i) minimizing the population in the state $|3\rangle$, (ii) minimizing the transfer time, and (iii) minimizing the pulse area. The equations for the open dynamics are obtained from a pure dephasing Markovian master equation ($\hbar = 1$),

$$\dot{\rho} = -i[H(t), \rho] + \sum_{i=1}^{3} \gamma_i (2\sigma_{ii}\rho\sigma_{ii} - \sigma_{ii}\rho - \rho\sigma_{ii}), \quad (8)$$

with $\gamma_i > 0$ representing dephasing rates associated with transverse relaxation processes. Without loss of generality, we set $\gamma_3 = 0.14$ and $\gamma_1 = \gamma_2 = 10^{-3}$, to account for larger dissipation in the excited state. We decomposed our density operator in real and imaginary parts, and passed the network a real-valued vector state: $\mathbf{z} = (\rho_{11}, \rho_{22}, \rho_{33}, \mathrm{Re}[\rho_{12}], \mathrm{Im}[\rho_{12}], \mathrm{Re}[\rho_{13}], \mathrm{Im}[\rho_{13}], \mathrm{Re}[\rho_{23}], \mathrm{Im}[\rho_{23}])^T$. The set of differential equations for the components of $\mathbf{z}$ is given in [81].

In Fig. 4-(a) we show the evolution of the population in the Λ-system and the predicted NN solutions for the control fields $\Omega_{s,p}(t)$. Note that our PINN successfully delivers a population transfer method with smooth pulses. Furthermore, it attempts to implement a counterintuitive sequence, turning on the Stoke pulse Ω_s (red-solid) at the same time that the pump field Ω_p (blue-dashed)— for a genuine counterintuitive sequence like STIRAP, Stokes pulse precedes the pump pulse. This is remarkable considering that the PINN has no knowledge about QC theory or the relevance of following a dark state evolution. It is worthwhile noticing that the Stoke pulse shown in the inset of Fig. 4-(a) triggers the $|2\rangle \leftrightarrow |3\rangle$ transition, which in STIRAP serves the purpose of preparing a dark state [85], since initially, all the population is in state $|1\rangle$.

For completeness, we depart from the polarized initial state $|1\rangle$ and focus on a more general initial state given by $\rho(0) = \sigma_{11}/2 + \sigma_{22}/2 + \epsilon(\sigma_{12} + \sigma_{21})/2$. For $\epsilon = 0$, we end up with a fully mixed state (without quantum coherence), while $\epsilon = 1$ provides a balanced coherent state. It is worth noting that neither STIRAP nor the other sequences are designed to transfer population from these initial states. Thus, adapting these sequences for the new purpose will demand further calculations. However, our PINN can handle this new task without changing the network's architecture, showing that PINNs provide a general and adaptive framework for inverse design. We focus on small deviations of $\epsilon = 1$. Designing a deep learning approach that handles arbitrary initial polarization is an interesting extension of the network, and it is left to future work. In Figs. 4-(b) and -(c) we show the population transfer and the corresponding pulse sequences for $\epsilon = 1$ and $\epsilon = 0.7$, respectively. Note
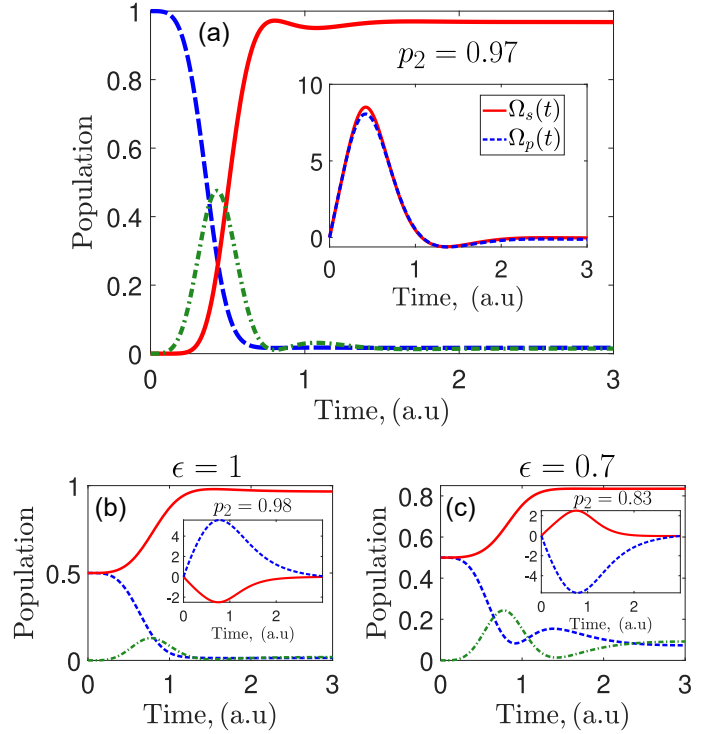

FIG. 4. (a) PINN successfully transfers population from the initial state $\rho(0) = |1\rangle\langle 1|$ to the target state $|2\rangle\langle 2|$ with probability $p_2 = \mathrm{Tr}[\rho\sigma_{22}]$. (b) The PINN allows us to polarize the system starting from a coherent ($\epsilon = 1$) and quasi-thermal state ($\epsilon = 0.7$). The architecture of the NN includes 5 hidden layers of 150 neurons and it is optimized over 2×10^4 training epochs with learning rate 8×10^{-3}, $\eta = 0.2$ and $\chi = 2.8 \times 10^{-3}$ [81].

that the PINN updates the pulses to deliver good polarizations.

For a thorough benchmarking, we consider other methods used to find optimal control pulses besides STIRAP [48, 49], such as Stimulated Raman Exact Passage (STIREP) [97], Inverse Engineering [89, 90] and Modified Superadiabatic Transitionless Driving (MOD-SATD) [20, 91]. For detailed calculations of these pulses, see [81]. In Table I we compare our results with the other pulse sequences. One can observe that PINN speeds up the population transfer with a high transferring rate. Moreover, the predicted control functions have the smallest area $\mathcal{A}$, as compared to the other methods. We remark that the regularization L_{reg} penalizes the fields for being too large and provides smooth functions. Thus, we can control the amplitudes of the fields and the pulse area to achieve a less power-consuming transfer, which can be crucial in practical implementations with low energy consumption requirements. Another practical advantage of our machine learning protocol is the robustness against two-photon detuning (δ). It is known that STIRAP deteriorates when increasing δ [86, 92]. Furthermore, the optimization for the other sequences with $\delta \neq 0$ is cumbersome and there is not much literature about it— to our best knowledge. To compare

TABLE I. The Table shows the population $p_2 = \text{Tr}[\rho\sigma_{22}]$, pulse area $\mathcal{A} = \int_0^{t_f} dt\sqrt{|\Omega_p(t)|^2 + |\Omega_s(t)|^2}$ and transfer time t_f (in arbitrary units). In parenthesis we report the values with $\Delta_1/2\pi = 0.2$ and $\delta/2\pi = 0.2$, the one- and two-photon detuning, respectively.

	PINN	STIRAP	STIREP	Inv. Eng.	MOD-SATD
p_2	0.97(0.93)	0.98(0.88)	0.98(0.91)	0.97(0.79)	0.98(0.89)
$\mathcal{A}$	7.3	128.6	53.3	19.8	50.0
t_f	2.0	35	9.4	3.0	13

the robustness of the earlier discovered pulse sequences, we also report in Table I the population transfer in the presence of two-photon detuning $\delta/2\pi = 0.2$. We stress that no training or further optimizations has been made to account for the new δ. Then, we observe that our PINN delivers a robust population transfer scheme. In [81] we show that the NN can be easily trained better to counteract the adversary effect of δ.

Finally, we extend our calculations to a four-level system and show that our PINN performs well against cross-talk to the newly added state [81], i.e., improves selectivity. Moreover, it generalizes the others Λ-optimized sequences and opens the path for a scalable method.

Conclusions.— In this letter, we introduced a physics-informed neural network to find optimal control functions in open quantum systems. We demonstrated a data-free deep learning approach that jointly solves the open dynamics of quantum systems and the inverse design of control functions. First, we applied this formalism to prepare a Gibbs state in a two-level system. Second, we applied it to state-to-state transfer in a three-level system. We found that the PINN provides a flexible method that adapts to different parameters, initial states, and power consumption requirements. We foresee an AI-assisted method that can be applied to a wide variety of dynamical systems.

* ariel.norambuena@umayor.cl
† raul.coto@umayor.cl

[1] P. Jamonneau, G. Hétet, A. Dréau, J.-F. Roch, and V. Jacques, Phys. Rev. Lett. 116, 043603 (2016).
[2] Y. Lin, J. Gaebler, F. Reiter, et al., Nature 504, 415–418 (2013).
[3] A. M. Brańczyk, P. E. M. F. Mendonça, A. Gilchrist, A. C. Doherty, and S. D. Bartlett, Phys. Rev. A 75, 012329 (2007).
[4] M. S. Blok, C. Bonato, M. L. Markham, D. J. Twitchen, V. V. Dobrovitski, and R. Hanson, Nat. Phys. 10,189 (2014).
[5] V. Montenegro, R. Coto, V. Eremeev, and M. Orszag, Phys. Rev. A 96, 053851 (2017).
[6] A. Bacciotti and L. Rosier, *Liapunov Functions and Stability in Control Theory* (Springer, London, 2001), Second Edition.
[7] Y-Q. Wang, Y. Wang, X. Zhao, et al. Quantum Inf Process 20, 404 (2021).
[8] J. Cui, R. van Bijnen, T. Pohl, S. Montangero and T. Calarco, Quantum Sci. Technol. 2, 035006 (2017).
[9] S. Cong, *Control of Quantum Systems: Theory and Methods* (Wiley, Singapore, 2014), First Edition.
[10] L. Viola, E. Knill, and S. Lloyd, Phys. Rev. Lett. **82**, 2417 (1999).
[11] L. Viola and E. Knill, Phys. Rev. Lett. 94, 060502 (2005).
[12] Xing-Long Zhen, Fei-Hao Zhang, Guanru Feng, Hang Li, and Gui-Lu Long Phys. Rev. A 93, 022304 (2016).
[13] J. Liu and S. Cong, 2011 9th IEEE International Conference on Control and Automation (ICCA), 318-323 (2011).
[14] S. L. Wu and W. Ma, Phys. Rev. A 105, 012204 (2022).
[15] X. M. Su and B. S. Ham, Phys. Rev. A 71, 013821 (2005).
[16] Y.-X. Du, Z.-T. Liang, W. Huang, H. Yan, and S.-L. Zhu, Phys. Rev. A 90, 023821 (2014).
[17] M. Anderlini, P. J. Lee, B. L. Brown, J. Sebby-Strabley, W. D. Phillips, and J. V. Porto, Nature 448, 452 (2007).
[18] G. Calajó, M. J. A. Schuetz, H. Pichler, M. D. Lukin, P. Schneeweiss, J. Volz, and P. Rabl, Phys. Rev. A **99**, 053852 (2019).
[19] D. Tancara, A. Norambuena, R. Peña, G. Romero, F. Torres, and R. Coto, Phys. Rev. A **103**, 053708 (2021).
[20] B. B. Zhou, A. Baksic, H. Ribeiro, C. G. Yale, F. J. Heremans, P. C. Jerger, A. Auer, G. Burkard, A. A. Clerk, and D. D. Awschalom, Nature Phys. 13, 330–334 (2017).
[21] Jiazhao Tian, Tianyi Du, Yu Liu, Haibin Liu, Fangzhou Jin, Ressa S. Said, and Jianming Cai Phys. Rev. A 100, 012110 (2019).
[22] D. Leibfried, R. Blatt, C. Monroe, and D. Wineland, Rev. Mod. Phys. 75, 281 (2003).
[23] G. Morigi, J. Eschner, C. Cormick, Y. Lin, D. Leibfried, and D. J. Wineland, Phys. Rev. Lett. 115, 200502 (2015).
[24] D. Press, T. D. Ladd, B. Zhanga, and Y. Yamamoto, Nature 456, 218–221 (2008).
[25] Georg Jäger, Daniel M. Reich, Michael H. Goerz, Christiane P. Koch, and Ulrich Hohenester Phys. Rev. A 90, 033628 (2014).
[26] C. Altafini and F. Ticozzi, IEEE Transactions on Automatic Control 57, 1898-1917 (2012)
[27] W. H. Fleming and R. W. Rishel, *Deterministic and Stochastic Optimal Control* (Springer-Verlag, New York, 1975).
[28] G. Carleo and M. Troyer, Science 355, 602 (2017).
[29] Z. Cai and J. Liu, Phys. Rev. B 97, 035116 (2018).
[30] K. Choo, G. Carleo, N. Regnault, and T. Neupert, Phys. Rev. Lett. 121, 167204 (2018).
[31] G. Torlai and R. G. Melko, Phys. Rev. Lett. 120, 240503 (2018)
[32] A. Nagy and V. Savona V, Phys. Rev. Lett. 122, 250501 (2019).
[33] M. J. Hartmann and G. Carleo, Phys. Rev. Lett. 122, 250502 (2019).
[34] F. Vicentini, A. Biella, N. Regnault, and C. Ciuti, Phys. Rev. Lett. 122, 250503 (2019).
[35] N. Yoshioka and R. Hamazaki, Phys. Rev. B 99, 214306 (2019).
[36] J. Carrasquilla and G. Torlai, PRX Quantum 2, 040201 (2021).

[37] R. Koch and J. L. Lado, Neural Network Enhanced Hybrid Quantum Many-Body Dynamical Distributions, Phys. Rev. Research 3, 033102 (2021).

[38] B. Gardas, M. M. Rams, and J. Dziarmaga, Phys. Rev. B 98, 184304 (2018).

[39] Z. Liu, L.-M. Duan, and D.-L. Deng, Phys. Rev. Research 4, 013097 (2022).

[40] M. Reh, M. Schmitt, and M Gärttner, Phys. Rev. Lett. 127, 230501 (2021).

[41] D. Luo, Z. Chen, J. Carrasquilla, and B. K. Clark, Phys. Rev. Lett. 128, 090501 (2022).

[42] P. P. Mazza, D. Zietlow, F. Carollo, S. Andergassen, G. Martius, and I. Lesanovsky, Phys. Rev. Research 3, 023084 (2021).

[43] W.Wu and Ze-Zhou Zhang, Sci Rep 11, 7188 (2021).

[44] K.-J. Boller, A. Imamoğlu, and S. E. Harris, Phys. Rev. Lett. 66, 2593 (1991).

[45] M. Fleischhauer, A. Imamoglu, and J. P. Marangos, Rev. Mod. Phys. 77, 633 (2005).

[46] E. Arimondo and G. Orriols, Lett. al Nuovo Cim. 17, 333–338 (1976).

[47] I. V. Jyotsna and G. S. Agarwal, Phys. Rev. A, 52, 3147 (1995).

[48] J. R. Kuklinski, U. Gaubatz, F. T. Hioe, and K. Bergmann, Phys. Rev. A 40, 6741(R) (1989).

[49] K. Bergmann, H. Theuer, and B. W. Shore, Rev. Mod. Phys.70, 1003 (1998).

[50] M. Y. Niu, S. Boixo, V. N. Smelyanskiy, and H. Neven, npj Quantum Inf 5, 33 (2019).

[51] Tangyou Huang, Yue Ban, E. Ya. Sherman, and Xi Chen, Phys. Rev. Applied 17, 024040 (2022).

[52] D. Castaldo, M. Rosa, and S. Corni, Phys. Rev. A 103, 022613 (2021).

[53] Thomas Fösel, Petru Tighineanu, Talitha Weiss, and Florian Marquardt, Phys. Rev. X 8, 031084 (2018).

[54] Y. X. Zeng, J. Shen, S. C. Hou, T. Gebremariam, C. Li, Physics Letters A 384, 126886 (2020).

[55] J. Brown, P. Sgroi, L. Giannelli, G. S. Paraoanu, E. Paladino, G. Falci, M. Paternostro, and A. Ferraro, New J. Phys. 23, 093035 (2021).

[56] V. V. Sivak, A. Eickbusch, H. Liu, B. Royer, I. Tsioutsios, and M. H. Devoret, Phys. Rev. X 12, 011059 (2022).

[57] F. Schindler, N. Regnault, and T. Neupert, Phys. Rev. B 95, 245134 (2017).

[58] J. B. Rigo and A. K. Mitchell, Phys. Rev. B 101, 241105(R) (2020).

[59] A. Borin and D. A. Abanin, Phys. Rev. B 101, 195141 (2020).

[60] X. Fang, K. Kruse, T. Lu, and J. Wang, Rev. Mod. Phys. 91, 045004 (2019).

[61] C. Letellier, I. Sendiña-Nadal, E. Bianco-Martinez, and M. S. Baptista, Sci Rep 8, 3785 (2018).

[62] A. Hannachi, Phys. Rev. E 60, 429 (1999).

[63] A. Tacchella, D. Mazzilli, and L. A. Pietronero, Nature Phys 14, 861–865 (2018).

[64] S. Denisov, J. Klafter, and M. Urbakh, Phys. Rev. E 66, 046203 (2002).

[65] D. Harnack, E. Laminski, M. Schünemann, and K. R. Pawelzik, Phys. Rev. Lett. 119, 098301 (2017).

[66] Melko2019, Nagy2019 R. G. Melko, G. Carleo, J. Carrasquilla, and J. I. Cirac, Nat. Phys. 15, 887–892 (2019).

[67] C. K. Lee, P. Patil, S. Zhang, and C. Y. Hsieh, Phys. Rev. Research 3, 023095 (2021).

[68] M. Raissi, P. Perdikaris, G.E. Karniadakis, Journal of Computational Physics 378, 686-707 (2019).

[69] G. E. Karniadakis, I. G. Kevrekidis, L. Lu, P. Perdikaris, S. Wang, and L. Yang, Nat Rev Phys 3, 422–440 (2021).

[70] J. A. Sirignano, K. Spiliopoulos, Journal of Computational Physics 375, 1339-1364 (2018).

[71] S. Zeng, Z. Zhang, Q. Zou, Journal of Computational Physics 463, 111232 (2022).

[72] D. Pfau, J. Spencer, A. G. D. G. Matthews, W. M. C. Foulkes, Phys. Rev. Research 2, 033429 (2020).

[73] M. Angeli, G. Neofotistos, M. Mattheakis, E. Kaxiras, Chaos, Solitons & Fractals 154, 111621, 2021.

[74] S. A. Desai, M. Mattheakis, D. Sondak, P. Protopapas, and S. J. Roberts Phys. Rev. E 104, 034312 (2021).

[75] K. Hornik, Neural Networks 4, 251–257 (1991).

[76] M. Mattheakis, D. Sondak, A. Dogra, P. Protopapas, Phys. Rev. E (accepted for publication).

[77] D. P. Kingma, J. Ba, CORR (2014)

[78] A. Paszke, S. Gross, S. Chintala, G. Chanan, E. Yang, Z. Devito, Z. Lin, A. Desmaison, L. Antiga, A. Lerer, NeurIPS (2017).

[79] D. Ran, Wu-Jiang Shan, Zhi-Cheng Shi, Zhen-Biao Yang, J. Song, and Y. Xia, Phys. Rev. A 101, 023822 (2020).

[80] R. Sagastizabal, S. P. Premaratne, B.A Klaver, et al. npj Quantum Inf 7, 130 (2021).

[81] See Supplemental Material.

[82] J. L Sørensen, D. Møller, T. Iversen, J. B. Thomsen, F. Jensen, P. Staanum, D. Voigt and M. Drewsen, New J. Phys. 8, 261 (2006).

[83] T. Yamamoto, Yu. A. Pashkin, O. Astafiev, Y. Nakamura, and J. S. Tsai, Demonstration of Conditional Gate Operation Using Superconducting Charge Qubits, Nature 425, 941 (2003).

[84] F. J. González and R. Coto, Quantum Sci. Technol. 7, 025015 (2022).

[85] R. Coto, V. Jacques, G. Hétet, and J. R. Maze, Phys. Rev. B 96, 085420 (2017).

[86] V.I. Romanenko and L.P. Yatsenko, Optics Comm. 140, 231 (1997,).

[87] Luigi Giannelli and Ennio Arimondo, Phys. Rev. A, 89, 033419 (2014).

[88] X. Chen, I. Lizuain, A. Ruschhaupt, D. Guéry-Odelin, and J. G. Muga, Phys. Rev. Lett. 105, 123003 (2010).

[89] X. Chen and J. G. Muga, Phys. Rev. A 86, 033405 (2012).

[90] Y.-Z. Lai, J.-Q. Liang, H. J. W. Müller-Kirsten, and J.-G. Zhou, Phys. Rev. A 53, 3691 (1996).

[91] A. Baksic, H. Ribeiro, and A. A. Clerk, Phys. Rev. Lett. 116, 230503 (2016).

[92] V. V. Nikolay, A. A. Rangelov, B. W. Shore, and K. Bergmann, Klaas, Rev. Mod. Phys. 89, 015006 (2017).

[93] D. Guéry-Odelin, A. Ruschhaupt, A. Kiely, E. Torrontegui, S. Martínez-Garaot, J. G. Muga, J. G., Rev. Mod. Phys. 91, 045001 (2019).

[94] H. Sun, N. Xu, S. Fan, and M. Liu, Annals of Physics 418, 168200 (2020).

[95] X. Chen, E. Torrontegui, and J. G. Muga, Phys. Rev. A 83, 062116 (2011).

[96] A. Kiely and A. Ruschhaupt, J. Phys. B: At. Mol. Opt. Phys. 47 115501 (2014).

[97] X. Laforgue, G. Dridi, and S. Guérin, Phys. Rev. A 105, 032807 (2022).

[98] We performed numerical simulations and observed no difference with the one-photon detuning.

Supplemental Material: Physics-informed neural networks for quantum control

Control and dynamical analysis in a two-level system

For the two-level system, we use the following loss function

$$L = ||\dot{\mathbf{x}} - A(\lambda, \mathbf{u}(t))\mathbf{x}||^2 + ||\mathbf{x} - \mathbf{x}_d||^2 + L_{\text{reg}}, \tag{9}$$

where $\mathbf{x}_d = (1/2, 1/2, 0, 0)^T$ is the desired control vector which correspond to ρ_d. The first, second, and third terms on the right-hand side of the above equation imposes the Markovian master equation, the state preservation problem ($\rho(t) \rightarrow \rho_d$) and the constraint for off-diagonal elements ($\rho_{eg} \rightarrow 0$). From the equation of motion $\dot{\mathbf{x}} = A\mathbf{x}$ given in the section for the two-level system, we found:

$$\dot{x}_1 = \gamma_e - 2\Gamma x_1 - 2\omega_x x_4, \tag{10}$$

$$\dot{x}_3 = -\Gamma x_3 - (2\omega_z + \xi(t)) x_4, \tag{11}$$

$$\dot{x}_4 = -\omega_x + 2\omega_x x_1 + (2\omega_z + \xi(t)) x_3 - \Gamma x_4, \tag{12}$$

where we have used $x_1 + x_2 = 1$ ($\text{Tr}(\rho) = 1$) and $\Gamma = (\gamma_{\text{abs}} + \gamma_{\text{em}})/2$. First, we can analyze the steady state which implies that solutions satisfy $\dot{x}_i = 0$ ($i = 1, 2, 3$). From numerical calculations using the PINN we found that $\xi(t)$ converges to a stable value, then we can asseverate that the steady state for ξ exist. Let us define x_i^{ss} and ξ^{ss} as the steady state solutions, from equations (10)-(12), we obtain:

$$\begin{pmatrix} 2\Gamma & 0 & 2\omega_x \\ 0 & \Gamma & 2\omega_z + \xi^{\text{ss}} \\ 2\omega_x & 2\omega_z + \xi^{\text{ss}} & -\Gamma \end{pmatrix} \begin{pmatrix} x_1^{\text{ss}} \\ x_3^{\text{ss}} \\ x_4^{\text{ss}} \end{pmatrix} = \begin{pmatrix} \gamma_e \\ 0 \\ \omega_x \end{pmatrix}. \tag{13}$$

By solving the above linear system, we get the following analytical solutions in terms of the steady-state ξ^{ss}

$$x_1^{\text{ss}} = \frac{\gamma_{\text{em}}}{\gamma_{\text{em}} + \gamma_{\text{abs}}} + \frac{4w_x^2(\gamma_{\text{abs}} - \gamma_{\text{em}})}{(\gamma_{\text{abs}} + \gamma_{\text{em}}\Delta(\xi^{\text{ss}}))}, \tag{14}$$

$$x_3^{\text{ss}} = \frac{4w_x(\gamma_{\text{abs}} + \gamma_{\text{em}})(2w_z + \xi^{\text{ss}})}{(\gamma_{\text{abs}} - \gamma_{\text{em}})\Delta(\xi^{\text{ss}})}, \tag{15}$$

$$x_4^{\text{ss}} = -\frac{2w_x(\gamma_{\text{abs}} - \gamma_{\text{em}})}{\Delta(\xi^{\text{ss}})}, \tag{16}$$

$$\Delta(\xi^{\text{ss}}) = (\gamma_{\text{abs}} + \gamma_{\text{em}})^2 + 8w_x^2 + 16w_z^2 + 16w_z\xi^{\text{ss}} + 4(\xi^{\text{ss}})^2. \tag{17}$$

For the particular case $w_x = 1$, $w_z = 2$, $\gamma_{\text{abs}} = 0.1$, and $\gamma_{\text{em}} = 0.3$ it follow that

$$x_1^{\text{ss}} = \frac{3}{4} - \frac{25}{2\Delta(\xi^{\text{ss}})}, \quad x_3^{\text{ss}} = -\frac{25(\xi^{\text{ss}} + 4)}{\Delta(\xi^{\text{ss}})}, \quad x_4^{\text{ss}} = -\frac{5}{2\Delta(\xi^{\text{ss}})}, \quad \Delta(\xi^{\text{ss}}) = 451 + 200\xi^{\text{ss}} + 25(\xi^{\text{ss}})^2. \tag{18}$$

Therefore, since the target state is defined as $\rho_d = (1/2)(|e\rangle\langle e| + |g\rangle\langle g|)$, or equivalently $x_d = (1/2, 1/2, 0, 0)^T$, we note that in order to obtain $x_3^{\text{ss}} = 0$ it is necessary to have $\xi^{\text{ss}} = -4$, as is shown in the inset of Figure. 3. In order to corroborate this previous observations rigorously, we impose that the steady state must minimize the function $f(\xi) = 1 - F(\rho(\xi), \sigma)$, where $\sigma = (1/2)(|e\rangle\langle e| + |g\rangle\langle g|)$ is the target state, $F(\rho, \sigma) = [\text{Tr}(\rho^{1/2}(t)\rho_d\rho^{1/2}(t))]^2$ is the quantum fidelity, and $\rho(\xi^{ss})$ is the steady state density matrix for ξ^{ss}, and is given by

$$\rho(\xi^{\text{ss}}) = \begin{pmatrix} x_1^{\text{ss}} & x_3^{\text{ss}} + ix_4^{\text{ss}} \\ x_3^{\text{ss}} - ix_4^{\text{ss}} & x_2^{\text{ss}} \end{pmatrix}, \tag{19}$$

where $x_2^{\rm ss} = 1 - x_1^{\rm ss}$. By emplying a nonlinear optimization package of MATLAB we minimize $f(\xi) = 1 - F(\rho(\xi), \sigma)$ over all possible values of $\xi^{\rm ss}$. We obtain

$$\min_{\xi^{\rm ss}}(1 - F(\rho(\xi), \sigma)) \quad \longrightarrow \quad \xi^{\rm ss} = -4, \quad \text{and} \quad F(\rho(-4), \sigma) = 0.9988. \tag{20}$$

By using the value $\xi^{\rm ss} = -4$, we obtain the best performance for the steady state solution in terms of the quantum fidelity ($F \approx 1$), which implie that $x_1^{\rm ss} = 0.549$, $x_3^{\rm ss} = 0$, and $x_4^{\rm ss} = 0.049$.

Energy efficiency of the control scheme

Let us consider a general Markovian open quantum system described by the master equation ($\hbar = 1$)

$$\dot{\rho} = -i[H_0 + H_c(t), \rho] + \mathcal{L}(\rho), \tag{21}$$

where H_0 and $H_c(t)$ are the bare and control Hamiltonians, respectively. Here, $\mathcal{L}(\rho)$ describes the loss term in the Lindblad master equation. Then, the average energy of the system can be defined as $\langle E \rangle = \text{Tr}(H(t)\rho)$, with $H(t) = H_0 + H_c(t)$. The average power can be written as

$$\frac{dU}{dt} = \text{Tr}(\dot{H}(t)\rho(t)) + \text{Tr}(H(t)\dot{\rho}(t)) = \text{Tr}(\dot{H}_c(t)\rho(t)) + \text{Tr}(H(t)\dot{\rho}) = \dot{W}(t) + \dot{Q}. \tag{22}$$

The term $\dot{W} = \text{Tr}(\dot{H}_c(t)\rho(t))$ is the power done by the system and $\dot{Q} = \text{Tr}(H(t)\dot{\rho})$ is the rate of heat induced by the reservoir. Thus, by direct integration we obtain the expression for the work $W(t)$ and heat $Q(t)$:

$$W(t) = \int_0^t \text{Tr}(\dot{H}_c(t)\rho(t)) \, d\tau, \quad Q(t) = \int_0^t \text{Tr}(H(t)\dot{\rho}) \, d\tau. \tag{23}$$

The time-dependent Hamiltonian competes with the heat flow induced by the environment. Therefore, we define $\eta = |W(t)/Q(t)|$ as the fraction of work done over the system compared to the internal heat that enters the system.
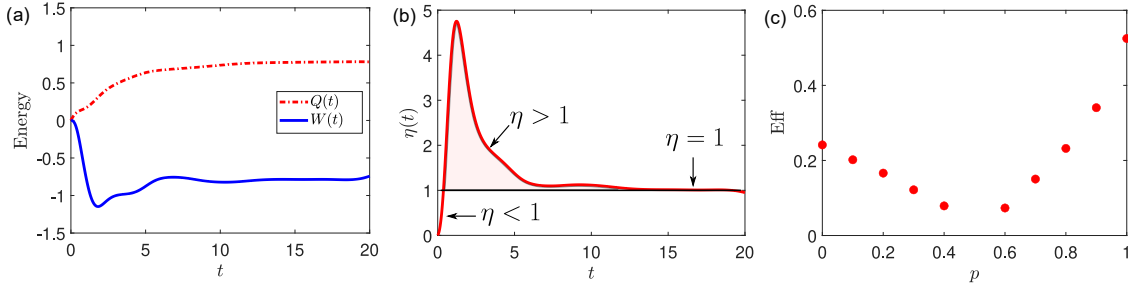

FIG. 5.

For the particular case of the two-level system presented in the main text, the work is given by

$$W(t) = \int_0^t \dot{\xi}(\tau)\rho_{ee}(\tau) \, d\tau, \tag{24}$$

where $\xi(t)$ is the control field. As $\rho_{ee} > 0$ and $\dot{\xi}$ is extremely negative at the beginning of the dynamics, we get that $-W > 0$. In Figure 5(a) we plot the ratio the quantities $Q(t)$ and $W(t)$ for the two-level system. Also, in Figure 5(b) we show the temporal behavior of $\eta(t) = |W(t)/Q(t)|$ for the same parameters used in Figure. 3. We note that we must apply a large quantity of work to overcome the effect of the internal heat. However, as time increases, the ratio η converges to 1, showing that the applied work compensates for undesired heat effects. Consequently, the system reaches a stable and free-losses state, which is required to preserve the state over time.

Now, we shall elaborate on a measure to quantify the efficiency of the control protocol in terms of energy considerations. By analyzing Figure 5(b), we note that an efficient quantum control solution can be recognized as the one that minimizes the colored area for the curve $\eta - 1$ for $\eta > 1$. In other words, if we control a quantum system without inverting a large quantity of energy, then $W_{\text{app}} \approx Q$, and therefore $\eta > 1$ only in a short time domain. Let us define the integral, $I_1 = \int_{\eta>1}(\eta(\tau) - 1)\, d\tau$ as a measure of the region where $\eta > 1$. In the best scenario, $I_1 = 0$, implying that the energy efficiency will be equal to one. In addition, the total area of the curve η will be represented by $I_2 = \int \eta(\tau)\, d\tau$. Based on these observations, we define the energy efficiency over the whole process as $\text{Eff} = 1 - I_1/I_2$, or equivalently

$$
\text{Eff} = 1 - \frac{\displaystyle\int_{\eta>1} (\eta(\tau) - 1)\, d\tau}{\displaystyle\int \eta(\tau)\, d\tau}, \quad 0 \le \text{Eff} \le 1. \tag{25}
$$

Since of $I_1 < I_2$ (by construction) and $I_1 = 0$ is the minimum value, it follow that $0 \le \text{Ef} \le 1$. Using this definition we have that $\text{Eff} = 0$ ($\text{Ef} = 1$) is the worst (best) scenario. For the two-level system we obtain that $\text{Ef} = 0.5249$. Now, if we consider the initial state parametrization $\rho(0) = p|g\rangle\langle g| + (1 - p)|e\rangle\langle e|$, we can calculate the energy efficiency in terms of the mixing parameter $0 \le p \le 1$. In Figure 5(c), we plot the efficiency of the PINN for $p = \{0, 0.1, 0.2, 0.3, 0.4, 0.5, 0.6, 0.7, 0.8, 0.9, 1\}$. Note that the efficiency is not reported for $p = 0.5$ since in such a a case, the initial state is equal to the target state.

Control and dynamical analysis in a three-level system

As it was stated in the main text, our PINN only handles real-valued functions. Therefore, we rewrite the master equation using the state vector $\vec{z} = (\rho_{11}, \rho_{22}, \rho_{33}, \text{Re}[\rho_{12}], \text{Im}[\rho_{12}], \text{Re}[\rho_{13}], \text{Im}[\rho_{13}], \text{Re}[\rho_{23}], \text{Im}[\rho_{23}])^T$. Hence, the dynamical equations reads,

$$
\begin{aligned}
0 &= \dot{z}_1 + \Omega_p(t)z_7, \\
0 &= \dot{z}_2 + \Omega_s(t)z_9, \\
0 &= \dot{z}_3 - \Omega_p(t)z_7 - \Omega_s(t)z_9, \\
0 &= \dot{z}_4 + \delta z_5 + (\gamma_1 + \gamma_2)z_4 + \frac{\Omega_p(t)}{2}z_9 - \frac{\Omega_s(t)}{2}z_7, \\
0 &= \dot{z}_5 - \delta z_4 + (\gamma_1 + \gamma_2)z_5 + \frac{\Omega_p(t)}{2}z_8 - \frac{\Omega_s(t)}{2}z_6, \\
0 &= \dot{z}_6 + \Delta_1 z_7 + (\gamma_1 + \gamma_3)z_6 + \frac{\Omega_s(t)}{2}z_5, \\
0 &= \dot{z}_7 - \Delta_1 z_6 + (\gamma_1 + \gamma_3)z_7 + \frac{\Omega_p(t)}{2}z_3 - \frac{\Omega_p(t)}{2}z_1 - \frac{\Omega_s(t)}{2}z_4, \\
0 &= \dot{z}_8 - \delta z_9 + \Delta_1 z_9 + (\gamma_2 + \gamma_3)z_8 - \frac{\Omega_p(t)}{2}z_5, \\
0 &= \dot{z}_9 + \delta z_8 - \Delta_1 z_8 + (\gamma_2 + \gamma_3)z_9 - \frac{\Omega_p(t)}{2}z_4 - \frac{\Omega_s(t)}{2}z_2 + \frac{\Omega_s(t)}{2}z_3.
\end{aligned} \tag{26}
$$

We can define the loss function that accounts for the model as $L_{\text{model}} = \sum_{i=1}^{9} \|L_i\|^2$, where L_i are given by the right-hand side in Eq. (26). The control loss function comes from the target state, such that

$$
L_{\text{control}} = \eta \|z_2 - 1\|^2. \tag{27}
$$

It is well-known that the master equation in the Lindblad form ensures that the density matrix will be Hermitian, positive, semi-definite, and $\text{Tr}[\rho] = 1$. However, we found that enforcing the last constraint helps the PINN to find the best solution. Therefore, we add the following term to the loss function

$$
L_{\text{const}} = \eta_c(\|z_1\|^2 + \|z_3\|^2), \tag{28}
$$

which together with L_{control} enforces $\text{Tr}[\rho] = 1$. Finally we added a l_2-norm regularization $L_{\text{reg}} = \chi \sum_i \Omega_i^2$ that penalizes the control fields being too large and delivers smooth functions. Henceforth, the PINN tries to minimize the

overall loss function:

$$L = L_{\text{model}} + L_{\text{control}} + L_{\text{const}} + L_{\text{reg}}, \tag{29}$$

with a learning rate that amounts to 8×10^{-3}. The weights in L_{control}, L_{const} and L_{reg} ($\eta = 0.2$, $\eta_c = 0.1$ and $\chi = 2.8 \times 10^{-3}$, respectively) regulate the relevance of the control, constraint, and smoothness conditions comparing to the leading loss component L_{model}. These weights were adjusted by hand, without cross-validation. In Fig. 6 we show the Loss function of the training process corresponding to Fig. 4-(a) in the main text.
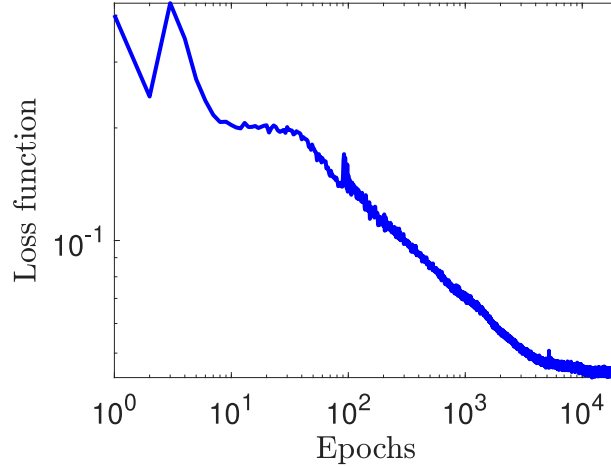

FIG. 6. Convergence of the loss function defined in Eq. (29).

Pulse sequences for controlling a Λ-system.

In this section, we detail some control protocols that exploit adiabaticity, shortcuts to adiabaticity, or inverse engineering. We aim to efficiently transfer population from an initially polarized state ($|1\rangle$) to a target state ($|2\rangle$) via an intermediary state ($|3\rangle$). To achieve this state-to-state transfer, two radiation fields are used to induce transitions $|1\rangle \leftrightarrow |3\rangle$ and $|2\rangle \leftrightarrow |3\rangle$, as shown in Fig. 2(b). In what follows, we provide a detailed derivation of each of these methods— some of them already addressed by us in Ref. [84] and included here to make the present paper self-contained. We remark that the optimization can be improved by increasing the control fields for most of these methods and our PINN. However, we restrict them to $\Omega_{s,p} \leq 10$ to fairly compare the methods. In Fig. 7 we compare all methods for the population transfer between the states $|1\rangle$ and $|2\rangle$.

Stimulated Raman Adiabatic Passage (STIRAP)

First, we consider a well-known protocol for adiabatic transfer dubbed Stimulated Raman Adiabatic Passage (STIRAP) [48, 49, 92]. Under the rotating wave approximation, the Hamiltonian for this system is given by,

$$H(t) = \delta\sigma_{22} + \Delta_1\sigma_{33} + \left(\frac{\Omega_p(t)}{2}\sigma_{31} + \frac{\Omega_s(t)}{2}\sigma_{32} + h.c.\right). \tag{30}$$

Hereafter, we set to zero the two-photon detuning $\delta = 0$ ($\Delta_1 = \Delta_2 = \Delta$). The eigenstates of the Hamiltonian are:

$$|\Phi_+\rangle = \sin\theta\sin\phi\,|1\rangle + \cos\phi\,|3\rangle + \cos\theta\sin\phi\,|2\rangle,$$
$$|\Phi_-\rangle = \sin\theta\cos\phi\,|1\rangle - \sin\phi\,|3\rangle + \cos\theta\cos\phi\,|2\rangle,$$
$$|\Phi_d\rangle = \cos\theta\,|1\rangle - \sin\theta\,|2\rangle, \tag{31}$$

with instantaneous eigenvalues $E_d = 0$ and $E_\pm(t) = \Delta/2 \pm \left(\Delta^2 + \Omega_p^2(t) + \Omega_s^2(t)\right)^{1/2}/2$. The mixing angles are defined through the relations

$$\tan\theta(t) = \frac{\Omega_p(t)}{\Omega_s(t)}, \quad \tan 2\phi(t) = \frac{\sqrt{\Omega_p^2(t) + \Omega_s^2(t)}}{\Delta}. \tag{32}$$

We note that the dark state ($|\Phi_d\rangle$) has no contribution from the excited state $|3\rangle$, so the population transfer from state $|1\rangle$ to state $|2\rangle$ is driven by the variation of the mixing angle $\theta(t)$. The latter implies that the Rabi frequencies $\Omega_p(t)$ and $\Omega_s(t)$ must be correlated. First, we note that $|\Phi_d\rangle$ coincides with $|1\rangle$ when $\theta(t) = 0$, which is obtained from $\Omega_p(t)/\Omega_s(t) \longrightarrow 0$. Second, the population transfer is completed when $|\Phi_d\rangle$ coincides with $|2\rangle$ ($\theta(t) = \pi/2$), that is obtained from $\Omega_p(t)/\Omega_s(t) \longrightarrow \infty$. Hence, the population transfer is attained with a counterintuitive pulse order, i.e. $\Omega_s(t)$ precedes $\Omega_p(t)$.

As mentioned above, the STIRAP protocol follows an adiabatic evolution, usually slower than superadiabatic control protocols. Therefore, we now focus on three different modifications to STIRAP that use superadiabatic corrections [87, 88, 93, 94], inverse engineering [89, 90] and counteradiabatic approach [91].

Inverse Engineering

Inverse engineering is one of the protocols that achieves high fidelity in shorter times. The main goal is to design the optimal control pulses $\Omega_p(t)$ and $\Omega_s(t)$. To determine these control fields, an invariant operator $I(t)$ is used, which satisfies the equation [89, 90],

$$\frac{\partial I(t)}{\partial t} + \frac{1}{i\hbar}[I(t), H_0(t)] = 0. \tag{33}$$

The condition $\Delta_1 = 0$ yields the following operator ($\hbar = 1$),

$$I(t) = \frac{\Omega_0}{2} \begin{pmatrix} 0 & \Xi(t) & \Upsilon(t) \\ \Xi(t) & 0 & \Xi(t) \\ \Upsilon^*(t) & \Xi(t) & 0 \end{pmatrix}, \tag{34}$$

with $\Xi(t) = \cos\gamma(t)\sin\beta(t)$ and $\Upsilon(t) = -i\sin\gamma(t)$. The time-dependent auxiliary parameters $\gamma(t)$ and $\beta(t)$ satisfy the following equations [95],

$$\frac{d\gamma(t)}{dt} = \frac{1}{2}(\Omega_p(t)\cos\beta(t) - \Omega_s(t)\sin\beta(t)),$$
$$\frac{d\beta(t)}{dt} = \frac{1}{2}\tan\gamma(t)(\Omega_s(t)\cos\beta(t) + \Omega_p(t)\sin\beta(t)). \tag{35}$$

From the above equations one can find the optimal control fields as

$$\Omega_s(t) = 2\left(\frac{d\beta(t)}{dt}\cot\gamma(t)\cos\beta(t) - \frac{d\gamma(t)}{dt}\sin\beta(t)\right),$$
$$\Omega_p(t) = 2\left(\frac{d\beta(t)}{dt}\cot\gamma(t)\sin\beta(t) + \frac{d\gamma(t)}{dt}\cos\beta(t)\right). \tag{36}$$

Henceforward, we shall consider different Ansatzs for the auxiliary parameters $\gamma(t)$ and $\beta(t)$.

Ansatz 1: For simplicity, we choose $\gamma(t) = \epsilon$ and $\beta(t) = \pi t/2t_f$ [89], that leads to

$$\Omega_s(t) = \frac{\pi}{t_f}\cot\epsilon\cos\left(\frac{\pi t}{2t_f}\right),$$
$$\Omega_p(t) = \frac{\pi}{t_f}\cot\epsilon\sin\left(\frac{\pi t}{2t_f}\right). \tag{37}$$

For the numerical calculations we set $\epsilon = 0.05$ and $t_f = 10$.

Ansatz 2: We choose the polynomial solution introduced in Ref. [89],

$$\beta(t) = \sum_{j=0}^{3} b_j t^j, \qquad \gamma(t) = \sum_{j=0}^{4} a_j t^j, \tag{38}$$

where the coefficients b_j and a_j are determined from the initial conditions

$$\gamma(0) = \epsilon, \quad \dot{\gamma}(0) = 0, \quad \gamma(t_f) = \epsilon, \quad \dot{\gamma}(t_f) = 0, \quad \gamma(t_f/2) = \delta,$$
$$\beta(0) = 0, \quad \dot{\beta}(0) = 0, \quad \beta(t_f) = \frac{\pi}{2}, \quad \dot{\beta}(t_f) = 0. \tag{39}$$

To obtain an optimal and fast population transfer we set $\epsilon = 0.02$, $\delta = \pi/10$ and $t_f = 3$. We show our results for this ansatz in Table I in the main text.

Ansatz 3: We choose the solution proposed in Ref. [96], that achieves successful population transfer in the presence of unwanted transitions. The parameters are,

$$\gamma(t) = -\frac{8(\pi - 2d_0)}{T^4}t^4 + \frac{2(7\pi - 16d_0 + T)}{T^3}t^3 - \frac{5\pi - 16d_0 + 3T}{T^2}t^2 + t,$$
$$\beta(t) = -\pi\left(\frac{t}{T}\right)^3 + \frac{1}{2}(2\pi d_1 + 3\pi)\left(\frac{t}{T}\right)^2 + \left(-\frac{1}{2}(2\pi d_1 + 3\pi + \frac{3\pi}{2})\right)\frac{t}{T} + d_1 \sin\left(\frac{\pi t}{T}\right), \tag{40}$$

where $d_0 = 1.8$, $d_1 = 0.1$ and $T = 1$. While this ansatz works fine, we did not include it in Table I due to the large control field, which we could not decrease below 10 with a successful transfer rate.

Stimulated Raman Exact Passage (STIREP)

Recently, a new protocol combines inverse engineering and optimization methods [97]. Here, the control pulses are determined by trajectories $\tilde{\phi}$ and read,

$$\tilde{\Omega}_s = \Omega_s(t)/2\dot{\eta} = \cos\tilde{\phi}\sin\tilde{\theta} - \dot{\tilde{\phi}}\cos\tilde{\theta},$$
$$\tilde{\Omega}_p = \Omega_p(t)/2\dot{\eta} = -\cos\tilde{\phi}\cos\tilde{\theta} - \dot{\tilde{\phi}}\sin\tilde{\theta}, \tag{41}$$

with $\tilde{\phi} = \phi[\eta(t)]$. The trajectory $\tilde{\phi}$ is obtained by applying robust inverse optimization (RIO) [97], which optimizes a cost function represented by the total area of the two pulses and is given by $\mathcal{A}_t = 2\int_{\eta_i}^{\eta_f}|\dot{\eta}|\sqrt{\dot{\tilde{\phi}}^2 + \cos^2\tilde{\phi}}\,d\eta$. By using the Euler-Lagrange equations and the Lagrange Multipliers method we obtain the following differential equations for the trajectory,,

$$\dot{y}_1 = \dot{\tilde{\phi}}^{\pm} = y_2,$$
$$\dot{y}_2 = \ddot{\tilde{\phi}}^{\pm} = -(2y_2^2 + \cos^2\tilde{\phi}^{\pm})\tan\tilde{\phi}^{\pm} \pm (\lambda_0\sec\tilde{\phi}^{\pm}\lambda_1\sin\eta - \lambda_2\cos\eta)\left(y_2^2 + \cos^2\tilde{\phi}^{\pm}\right)^{3/2} = 0. \tag{42}$$

For the initial condition $\dot{\tilde{\phi}} = 0$ we end up with the Lagrange Multipliers $\lambda_0 = 0.394$, $\lambda_1 = -0.064$ and $\lambda_2 = 0.283$.

Modified Superadiabatic Transitionless Driving (MOD-SATD)

The MOD-SATD [91] protocol is a different alternative, which bypasses the adiabatic condition while counteracting the effect of the loss of adiabaticity. The fields in this protocol are parameterized according to [91]

$$\Omega_p(t) = -\Omega'(t)\sin\theta'(t),$$
$$\Omega_s(t) = \Omega'(t)\cos\theta'(t), \tag{43}$$

where $\theta'(t) = \theta(t) - \arctan[g_x(t)/(\Omega(t) + g_z(t))]$, $\Omega'(t) = \sqrt{[\Omega(t) + g_z(t)]^2 + g_x^2(t)}$, $\mu(t) = -\arctan[\dot{\theta}/(\Omega(t) + g(t)/\sigma_m)]$, $g_x(t) = \dot{\mu}$, $g_z(t) = -\Omega(t) - \dot{\theta}/\tan(\mu)$, $g(t) = A/\cosh(\zeta t)$ with $A = 1/40$, $\zeta = 9/(10\sigma_m)$ and $\sigma_m = 2.0$ μs. For the Gaussian fields considered in STIRAP one finds that [91]

$$\theta(t) = \arctan\left[\exp\left(t_d t/\sigma^2\right)\right],$$
$$\Omega(t) = \Omega_0\exp\left(-\frac{t^2 + t_d^2/4}{2\sigma^2}\right)\sqrt{2\cosh\left(\frac{t_d t}{\sigma^2}\right)}, \tag{44}$$
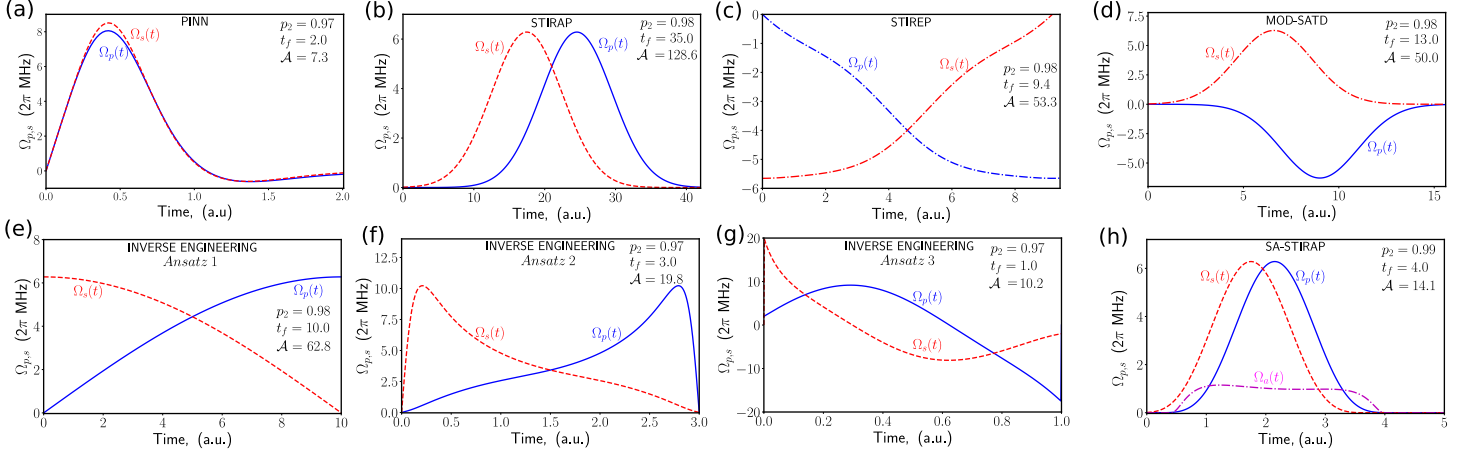
with $t_d = 6/5\sigma$ and $\Omega_0/2\pi = 1$ MHz.

FIG. 7. Comparing all methods for population transfer from state $|1\rangle$ to $|2\rangle$.

Superadiabatic STIRAP (SA-STIRAP)

For completeness, we also show the SA-STIRAP sequence. However, we do not consider it in the main text (Table I) because it relies on a pulse connecting states $|1\rangle$ and $|2\rangle$, which we have not allowed for our PINN.

The superadiabatic approximation requires an external control Hamiltonian $H_c(t)$ [87, 88, 94], such that

$$H_{sa}(t) = H(t) + H_c(t), \tag{45}$$

where $H(t)$ is the original Hamiltonian in Eq. (30). The superadiabatic correction reads ($\hbar = 1$),

$$H_c(t) = i \sum_{n=\pm,d} \left[|\partial_t \Phi_n(t)\rangle \langle \Phi_n(t)| - \langle \Phi_n(t)| \partial_t \Phi_n(t)\rangle |\Phi_n(t)\rangle \langle \Phi_n(t)| \right], \tag{46}$$

where $|\Phi_n\rangle$ are the eigenstates $H(t)$, as given in Eq. (31). After straightforward calculations we obtain the superadiabatic correction

$$H_c(t) = \frac{1}{2} \left(i\Omega_a(t)\sigma_{21} - i\Omega_a^*(t)\sigma_{12} \right), \tag{47}$$

with $\Omega_a(t) \equiv 2d\theta(t)/dt$, and $\theta(t)$ given in Eq. (32). Instead of Gaussian fields (as we used in the STIRAP protocol), here we use $\Omega_p(t) = \Omega_0 \sin^4(\pi(t-\tau)/T)$ and $\Omega_s(t) = \Omega_0 \sin^4(\pi t/T)$, with $\Omega_0/2\pi = 1$, $\tau = 0.1T$ and $T = 4$.

Optimization with two-photon detuning

The one-photon detuning does not have a detrimental role in the transfer protocol. For instance, it is known that it does not affect STIRAP in the adiabatic limit [92, 98]. In contrast, the two-photon detuning (δ) hurts the success in the population transfer [86, 92]. Back to STIRAP, neither the dark state nor the null eigenvalue are available, forcing variations in the sequence (or a total departure from it) to achieve a successful transfer. Our PINN, on the other hand, can be easily trained to counteract this effect. It only requires setting the new value of δ before the training process, and then the PINN automatically updates the weights in the optimization and delivers a population transfer probability with a final probability $p_2 = 0.94$, see Fig. 8. Furthermore, it is worth noticing that the pulse sequence found by the PINN does not experience a significant change. This means the sequence is robust without a subsequent optimization ($p_2 = 0.93$ in the main text). It is important to note that along the manuscript with have fixed the regularization parameter $\chi = 2.8 \times 10^{-3}$. However, decreasing it down to $\chi = 1 \times 10^{-3}$ will increase the control fields and deliver a population transfer with $p_2 = 0.97$.

Four-level system

The optimization of control pulses is, in general, system-dependent. This means that once we have the optimal pulse sequence for a Λ-system, the extension to a four-level system is not straightforward. For instance, the new system involves
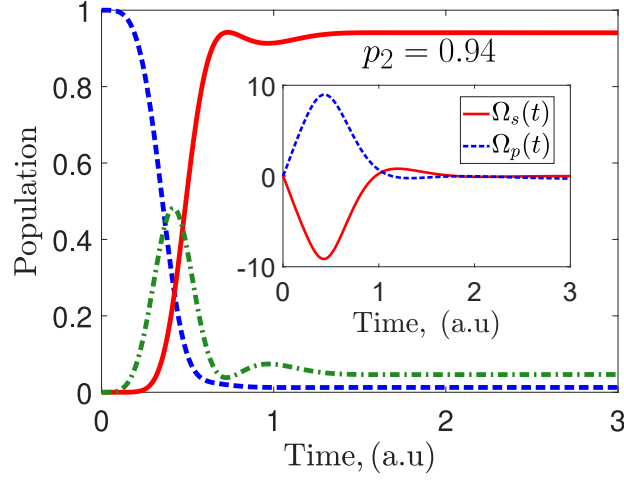
FIG. 8. Training the PINN considering one- ($\Delta_1/2\pi = 0.2$) and two-photon ($\delta/2\pi = 0.2$) detuning can easily improve the population transfer from $p_2 = 0.93$ to $p_2 = 0.94$.

more non-linear equations and the possibility of cross-talk to the newly added state. Henceforth, any analytical approach for optimization becomes a hard task. In this section, we show that our PINN can handle a four-level system without modification to the architecture of the network. Then, we feed the PINN with the new set of differential equations, and we add a new constraint in L_{const} (28) for the population in the fourth state $\|z_4\|^2$. Our goal is to train a PINN that succeeds in transferring population from state $|1\rangle$ to state $|2\rangle$, with, (i) minimizing the population in the lossy intermediary state ($|3\rangle$), (ii) minimizing the transfer time, (iii) minimizing the pulse area, and (iv) minimizing cross-talk to state $|4\rangle$. Note that the last condition was unnecessary for the three-level system and guarantees selectivity.

To begin with, we consider the Hamiltonian of the system in a multi-rotating frame and in the eigenstate basis ($\hbar = 1$),

$$\hat{H} = \delta\sigma_{22} + \Delta_3\sigma_{33} + \Delta_4\sigma_{44} + \frac{\Omega_p(t)}{2}\left(\sigma_{13} + \sigma_{14}\right) + \frac{\Omega_s(t)}{2}\left(\sigma_{23} - \sigma_{24}\right) + h.c., \tag{48}$$

where $\Omega_p(t)$ and $\Omega_s(t)$ are the Rabi frequencies of the control fields and σ_{ij} the ladder operators. The one-photon detunings are $\Delta_2 = (E_3 - E_2 - \omega_s)$, $\Delta_3 = (E_3 - E_1 - \omega_p)$, $\Delta_4 = (E_4 - E_1 - \omega_p)$ and the two-photon detuning is $\delta_2 = (\Delta_3 - \Delta_2)$. E_i are the eigenenergies and ω_p and ω_s are the frequency of the control fields. This Hamiltonian can be obtained from the interaction of a Nitrogen-Vacancy center with a Carbon-13 nuclear spin [84, 85]. In Fig. 9 we show the population transfer method.
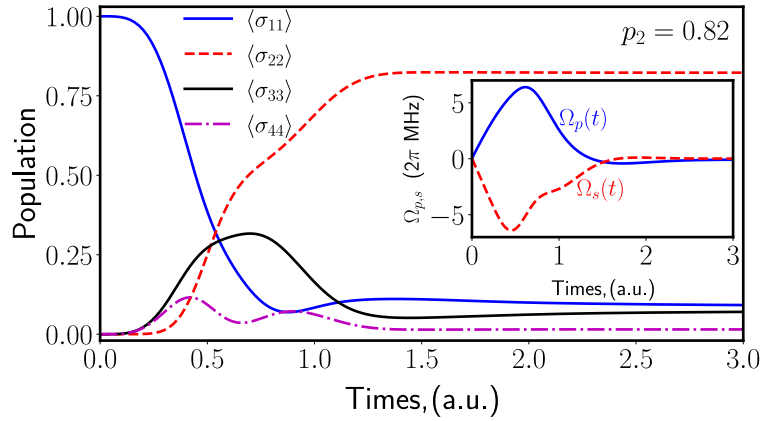

FIG. 9. PINN delivers a successful population transfer method that can be scaled to a four-level system without changing the network's architecture.